HYBRIDIZATION OF NUMERICALLY RIGOROUS TECHNIQUES WITH ASYMPTOTIC METHODS VIA THE USE OF THE GENETIC ALGORITHM AND PRONY'S METHOD

Raj Mittra and Tao Su

Electromagnetic Communication Lab
Department of Electrical Engineering
Pennsylvania State University
University Park, PA 16802-2705, USA
rajmittra@ieee.org

Radar scattering problems are often handled via asymptotic techniques, for instance the GTD or PTD, because the object size is too large to be amenable to analysis by numerically rigorous methods that are highly cpu-intensive. However, the asymptotic methods have two important drawbacks: (i) they lose accuracy as we attempt to approach the resonance range from above—hence their range of applicability is limited; (ii) diffraction coefficients are not conveniently available for many geometries of interest. Thus, currently, there exists a "no man's land," which is often difficult to cross, despite the recent advances in numerically efficient algorithms such as the Fast Multipole Method (FMM) and parallelized version of FDTD scheme that have enabled us to make a quantum leap into the regime of the problem sizes that can now be tackled numerically rigorously. The objective of this paper is to propose a hybridization technique—applicable to a class of RCS problems—that transitions from the numerically rigorous to asymptotic schemes in a smooth, seamless manner. The method is fundamentally different from the hybridization schemes that have been proposed in the past in the context of the Method of Moments , where attempts have been made to merge the subdomain basis functions, e.g., RWG types, with entire domain ones derived by using the Physical Optics (PO) type of approximation. Such approaches are difficult to implement in practice in a systematic manner, one that enables us to check the convergence and improve the accuracy of the solution.

The step-by-step method to be followed in an alternate approach that we propose in this work will now be described. We begin by analyzing the scattering characteristics of the object at low frequencies, and progressively transition through the resonance range, into the lower edge of the high frequency regime, where it becomes possible to express the far scattered fields in terms of contributions from a finite number of scattering centers. Next, we process the far field data in the transition frequency region (above resonance) for a fixed look angle, by repeatedly applying Prony's method over a relative narrow frequency window, and extracting the locations as well as weights of the scattering centers in each band. The third step is to employ the Genetic Algorithm (GA) and fit the frequency behaviors of the weights of the scattering centers as powers (fractional or integral, real or complex) of the wave number k. We then construct a representation of the scattered field as a function of k, which is similar in form to that we would derive for the far scattered field for the object if we were using asymptotic methods and had access to a functional representation of the diffraction coefficients associated with these centers. We test this representation by pushing further into the higher frequency range and verifying that the extrapolation procedure based on the above representation is sufficiently accurate. We then postulate that the representation would get progressively better as we move to even higher frequencies—well above the resonance region—and would smoothly transition into the asymptotic solution.

To illustrate the application of the technique described above, we apply the method to the problem of computing the back-scattering of a PEC cone. We begin by computing the scattered field by using the MoM in the frequency range of 1 to 3.8 GHz for the VV polarization. We then process the data using the method described above and verify the accuracy of the resulting scattering center model by comparing the scattered field predicted by this model with that computed via direct simulation. The comparison is shown in Fig. 1, where the blue curves represent the simulation data in frequency and time domains, respectively, in Figs. 1(a) and (b), while the red dashed curves in these plots are calculated by using the model. Good agreement between the two results is clearly evident from these plots. Note that we can identify three major scattering centers from the time-domain plot, and the scattering mechanisms corresponding to these centers, namely the tip diffraction, the edge diffraction and the creeping wave contribution, are illustrated in Fig. 2. The postulation of these mechanisms is based on the scattering physics as well as on the time delays associated with these centers.

Once we have completed the verification of the model, we can use it to extrapolate the scattered field to higher frequencies. The contributions of the major scattering centers are extrapolated to the C and X bands, centered at 6GHz

and 10 GHz, respectively. Table 1 shows the comparison of the RCS values calculated from the model and the measured data. The overall comparison is good, even though the simulation frequency used to derive the model is far below these two extrapolation frequency ranges, with the dimensions of the target being considerably more manageable at the lower frequencies from the point of view of numerical simulation, whereas they may be totally impractical to handle at the higher frequencies.

The scope and limitations of the approach will be pointed out during the course of the presentation, and methods for improving its accuracy by simultaneously processing angular and frequency sweep data (2-D *vs.* 1-D) will be suggested. Finally, extension to dielectric coated targets will also be discussed.

References:

[1] M. P. Hurst and R. Mittra, "Scattering center analysis via Prony's method," *IEEE Trans. Antennas Propagat.*, vol. 35, no. 8, pp. 986-988, Aug. 1987.

[2] L. C. Potter and R. L. Moses, "Attributed scattering centers for SAR ATR," *IEEE. Trans. Image Processing*, vol. 6, no. 1, pp. 79-91, Jan. 1997.

[3] Y. Wang and H. Ling, "Radar signature prediction using moment method codes via frequency extrapolation," *IEEE Trans. Antennas Propagat.*, vol. 47, no. 6, pp. 1008-1015, June 1999.

[4] J. Choi, N. Wang L. Peters, Jr. and P. Levy, "Near axial backscattering from finite cones," *IEEE Trans. Antennas Propagat.*, vol. 38, no. 8, pp. 1264-1272, Aug. 1990.

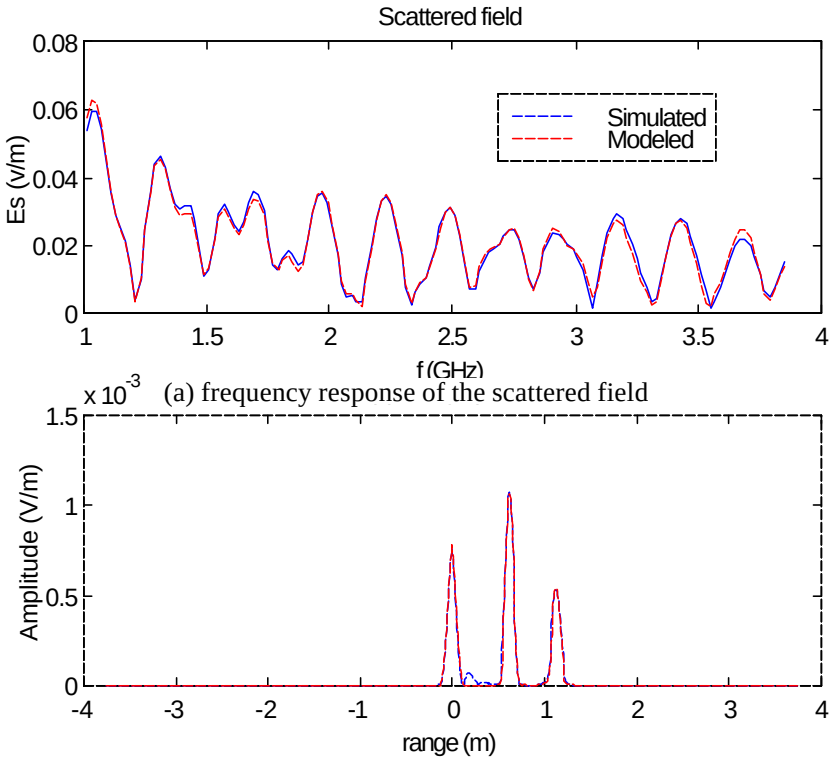

(b) time-domain response of the scattered field

Fig. 1. The scattering centered model is extracted from the simulated scattered field and optimized using GA. It agrees very well with the direct simulation in both frequency- and time-domain. The data is collected for VV-polarization at an incident angle of 60º from the tip.

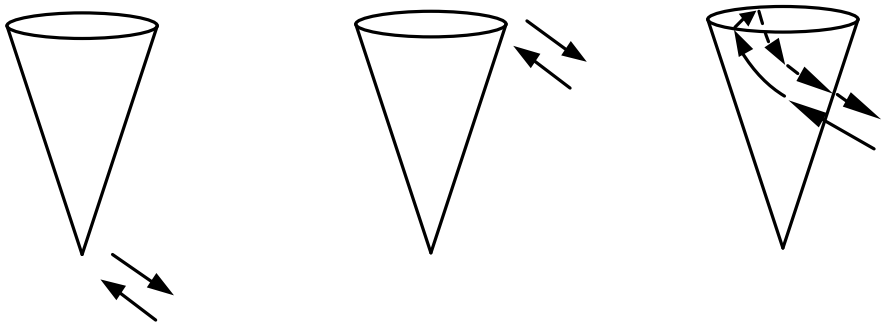

(a) tip diffraction (b) edge diffraction (c) creeping wave

Fig. 2. Three major scattering mechanisms are corresponding to the three scattering centers in Fig. 1, in that order.

Table. 1. Comparison of RCS (-dBsm) due to different mechanisms obtained from the hybrid method and the measurement data, VV-polarization
(hybrid method / measurement)

		Modeling		Extrapolation	
Angle	Mechanism	L	S	C	X
	Tip diffraction	29/28	29/28	28/27	28/28
30°	Edge diffraction	38/38	39/41	42/43	44/46
	Creeping wave	28/30	29/31	32/38	34/46
	Tip diffraction	29/29	29/29	28/29	27/29
45°	Edge diffraction	33/34	34/34	37/37	39/39
	Creeping wave	37/36	42/36	51/47	60/<55
	Tip diffraction	30/28	31/28	32/29	34/29
60°	Edge diffraction	26/26	27/27	29/30	32/33
	Creeping wave	34/32	42/41	55/<55	67/55
	Tip diffraction	23/22	23/23	23/24	23/26
75°	Edge diffraction	14/13	15/14	17/17	20/20
	Creeping wave	31/28	35/33	41/41	47/<55
	Tip diffraction	23/23	26/24	31/27	35/31
90°	Edge diffraction	11/10	12/12	14/14	17/17
	Creeping wave	38/28	42/29	49/34	55/44
	Tip diffraction	30/26	35/31	42/39	49/41
105°	Edge diffraction	18/18	19/19	21/22	23/24
	Creeping wave	41/44	49/36	35/48	31/<55
	Tip diffraction	36/34	38/44	42/45	46/48
120°	Edge diffraction	19/20	21/21	23/22	25/26
	Creeping wave	47/<55	48/<55	50/52	51/53